Available online at www.sciencedirect.com

ScienceDirect

Advances in Space Research 74 (2024) 3186–3200

ADVANCES IN SPACE RESEARCH (a COSPAR publication)

www.elsevier.com/locate/asr

Advances in Atom Interferometry and their Impacts on the Performance of Quantum Accelerometers On-board Future Satellite Gravity Missions

Alireza HosseiniArani [a,*], Manuel Schilling [b], Quentin Beaufils [c], Annike Knabe [a], Benjamin Tennstedt [a], Alexey Kupriyanov [a], Steffen Schön [a], Franck Pereira dos Santos [c], Jürgen Müller [a]

[a] Institute of Geodesy (IfE), Leibniz University Hannover, Schneiderberg 50, Hannover 30167, Germany
[b] Institute for Satellite Geodesy and Inertial Sensing, German Aerospace Center (DLR), Callinstraße 30B, Hannover 30167, Germany
[c] LNE-SYRTE, Observatoire de Paris, Université PSL, CNRS, Sorbonne Université, 61, avenue de l'Observatoire, Paris 75014, France

Received 10 April 2024; received in revised form 4 June 2024; accepted 21 June 2024
Available online 26 June 2024

Abstract

Recent advances in cold atom interferometry have cleared the path for space applications of quantum inertial sensors, whose level of stability is expected to increase dramatically with the longer interrogation times accessible in space. In this study, an in-orbit model is developed for a Mach–Zehnder-type cold-atom accelerometer. Performance tests are realized under different assumptions about the positioning and rotation compensation method, and the impact of various sources of errors on instrument stability is evaluated. Current and future advances for space-based atom interferometry are discussed, and their impact on the performance of quantum sensors on-board satellite gravity missions is investigated in three different scenarios: state-of-the-art scenario (expected to be ready to launch in 5 years), near-future (expected to be launched in the next 10 to 15 years) and far-future scenarios (expected for the next 20 to 25 years). Our results indicate that the highest sensitivity is achievable by positioning the electrostatic accelerometer at the center of mass of the satellite and the quantum accelerometer aside, on the cross-track axis of the satellite. We show that one can achieve a sensitivity level close to 5×10^{-10} m/s^2/$\sqrt{\text{Hz}}$ with the current state-of-the-art technology. We also estimate that in the near and far-future, atom interferometry in space is expected to achieve sensitivity levels of 1×10^{-11} m/s^2/$\sqrt{\text{Hz}}$ and 1×10^{-12} m/s^2/$\sqrt{\text{Hz}}$, respectively. A roadmap for improvements in atom interferometry is provided that would maximize the performance of future quantum accelerometers, considering their technical capabilities. Finally, the possibility and challenges of having ultra-sensitive atom interferometry in space for future space missions are discussed.

Keywords: Atom interferometry; CAI accelerometer; Quantum sensors; Quantum accelerometers; Inertial sensors; Satellite gravimetry; Satellite gravity missions

1. Introduction

1.1. Satellite gravity missions

Satellite gravimetry missions monitor the Earth's gravity field and its changes over time. Results from previous missions like GRACE(-FO) contributed to quantifying mass

* Corresponding author.
E-mail addresses: hosseiniarani@ife.uni-hannover.de (A. HosseiniArani), Manuel.Schilling@dlr.de (M. Schilling), quentin.beaufils@obspm.fr (Q. Beaufils), knabe@ife.uni-hannover.de (A. Knabe), tennstedt@ife.uni-hannover.de (B. Tennstedt), kupriyanov@ife.uni-hannover.de (A. Kupriyanov), schoen@ife.uni-hannover.de (S. Schön), franck.pereira@obspm.fr (F. Pereira dos Santos), mueller@ife.uni-hannover.de (J. Müller).

https://doi.org/10.1016/j.asr.2024.06.055
0273-1177/

variations related to climate change (Tapley et al., 2019; Humphrey et al., 2023; Scanlon et al., 2023) and brought new insights into processes of the Earth's interior (Mandea et al., 2020; Lecomte et al., 2023). But current solutions of the gravity field provided by these satellite gravity missions are limited in the very low degrees at C_{20} and, for times with only one operational accelerometer on two satellites, even at C_{30} (Loomis et al., 2020). These coefficients are thus typically replaced with satellite laser-ranging solutions.

The drift in low frequencies of the electrostatic accelerometers used limits the gravity field solution. Fig. 1 shows the amplitude spectral densities of three electrostatic accelerometers. Within a certain bandwidth, approximately between 10^{-3} Hz to 10^{-1} Hz, the spectrum is flat for all accelerometers. Similarly, below 10^{-3} Hz the ASD increases, most likely due to thermal effects on the accelerometer bias, for the three instruments. The upcoming GRACE-C (Gravity Recovery and Climate Experiment — Continuation) mission, to be launched by NASA and DLR in the late 2020s, will also employ electrostatic accelerometers similar to the GRACE-FO instrument. Therefore, we consider this instrument as our state-of-the-art electrostatic accelerometer. The requirements on the accelerometer for ESA's Next Generation Gravity Mission(NGGM; Massotti et al., 2021; Daras et al., 2023), expected to be launched in the first half of the 2030's, are more stringent. As an example, an electrostatic accelerometer in development at ONERA as a part of a hybrid accelerometer(Zahzam et al., 2022), which meets NGGM's requirements, is also shown in Fig. 1.

Accelerometers based on cold atom interferometry (CAI) are expected to feature a significantly reduced drift, and close to white noise in a wider frequency band. The fusion of a quantum and a classical accelerometer in a hybrid accelerometer combines the advantages of both technologies: the high data rate and low noise at high frequencies of the electrostatic accelerometer and the long term stability of a quantum accelerometer, with increased sensitivity due to longer interrogation times of the atom interferometer. The benefit hybridisation for gravity field missions has been shown, for example, in(Abrykosov et al., 2019). For the quantum accelerometer, the increased sensitivity comes at the cost of a data rate below1 Hz and consequently a lower bandwidth.This will be shown in the following sections.

Overall, the spatial resolution of current gravity field missions is limited to $> (400\,\mathrm{km})^2$ for a signal amplitude of 10 mm for typical monthly gravity field solutions. To address the needs of the scientific community, future satellite gravity missions shall target a resolution of $(200\,\mathrm{km})^2$ for an amplitude of 10 mm equivalent water height or even smaller (Pail et al., 2015; Wiese et al., 2022). This would allow, among others, more accurate measurements of the mass balance of smaller glaciers or sea level changes, as well as drought or flood predictions on a regional scale.

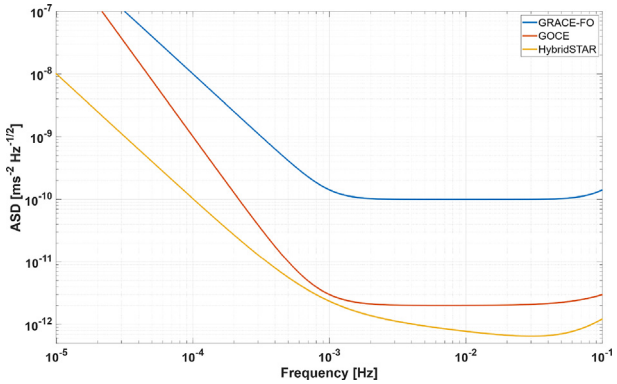

Fig. 1. ASD of electrostatic accelerometers of the GRACE-FO and GOCE mission (Touboul et al., 2016) and an electrostatic accelerometer currently in development as component of a hybrid accelerometer (HybridSTAR; Zahzam et al., 2022).

Potential technologies to overcome current limitations are, for example, improvements of electrostatic accelerometers by enhanced readout schemes (Dávila Álvarez et al., 2022; Kupriyanov et al., 2024), sensors based on atom interferometry (Lévèque et al., 2009) and combinations of classical and quantum accelerometers in a hybrid configuration (Zahzam et al., 2022). This work focuses on cold atom interferometry and hybrid concepts.

It should be stressed that temporal aliasing, primarily resulting from monthly sampling, constitutes, in practice, a significant source of error due to the inherent limitations in the modeling of high-frequency oceanic and atmospheric mass variations. This barrier could be overcome, though, by deploying satellite constellations, e.g., comprising two pairs of satellites in an optimized orbital configuration (Purkhauser et al., 2020). It is thus important to acknowledge that an optimized satellite constellation, coupled with a strategy for mitigating temporal aliasing errors, is essential to fully leverage the capabilities of improved instrumentation. However, the study of such satellite constellations lies beyond the scope of this paper and will be addressed in future studies.

1.2. Cold atom interferometry

Atom interferometry is a promising candidate technology for performing accelerometry in satellites as it allows the realisation of high-performance inertial sensors with a flat noise spectrum (Geiger et al., 2020). In such sensors, atoms in free fall are used as test masses. Their acceleration in the satellite frame is precisely measured by realizing an atom interferometer with sequences of laser pulses. Such light-pulse atom interferometers can be implemented in a number of different ways (seeAbend et al., 2020, for an overview), and only a brief introduction based on Kasevich and Chu (1991) is given here. The atom interferometer is implemented by three laser pulses acting either as beam splitters or mirror pulses. These laser pulses consist of two counter-propagating laser beams, whose frequency

difference is tuned in resonance with a two-photon Raman transition between the two hyperfine ground states of an alkali atom, ^{87}Rb in our case. The first pulse of light acts as a beam splitter for matter waves. It places the atom in a quantum superposition of two wave packets of different momenta that spatially separate after the pulse during a time interval T. A second light pulse inverts the momenta of the two wave packets. Finally, a beamsplitting pulse closes the interferometer after a further time interval T. The atom interferometer phase shift $\Delta\Phi$ depends on the projection of the acceleration a experienced by the atoms along the effective optical wave vector of the laser light $\vec{k}_{\text{eff}} = \vec{k}_1 - \vec{k}_2$ which is the difference between the optical wave vectors $\vec{k}_i$ of both laser beams. The leading order of the atom interferometer phase $\Delta\Phi$ is described by

$$\Delta\Phi = (2k_{\text{eff}}a)T^2 + \Phi_L \tag{1}$$

with the acceleration a and $k_{\text{eff}} = |\vec{k}_{\text{eff}}|$ now expressed in the direction of the counterpropagating laser beams. k_{eff} is also related to the photon momentum transfer induced by the Raman transitions. A factor 2 is added because of the double diffraction configuration of the atom interferometer expected in microgravity(Lévèque et al., 2009).

When the interferometer is operated in single diffraction, an arbitrary Raman laser phase Φ_L can be added to the last light pulse to scan the fringe pattern, or to operate the interferometer at mid-fringe ($\Delta\Phi = \pi/2$) as described in HosseiniArani et al. (2022). This mid-fringe operation enables the CAI-based quantum sensor to achieve the highest sensitivity to non-gravitational accelerations.. In double diffraction (Lévèque et al., 2009), this can be achieved by shifting the reference mirror's position, e. g.with a piezoelectric actuator.

In a satellite setting, the instrument can be used to measure the non-gravitational accelerations acting on the satellite. A three-axis instrument could also be implemented for geodesy applications but in this paper we focus on a single-axis quantum accelerometer oriented in the along-track (X-) direction. Eq. (1) describes a single-axis accelerometer phase shift in the absence of rotation of the satellite. A more complete version of this equation including the first-order effects of rotations is shown in Eq. (3) (Section 2.3).

Currently, the technology to operate a quantum accelerometer in space is still under development. While quantum gravimeters are available for terrestrial applications, including commercial instruments (Antoni-Micollier et al., 2022; Antoni-Micollier et al., 2024), space applications are in a much more experimental state. Experiments on sounding rockets demonstrated the generation of a Bose–Einstein Condensate in space with the MAIUS Experiment (Becker et al., 2018). The follow up missions MAIUS-2/3 are planned to perform differential acceleration measurements between two species of atoms to test the Einstein equivalence principle (Elsen et al., 2023). Additionally, NASA operates the Cold Atom Lab (CAL) onboard the International Space Station (Aveline et al., 2020) since 2018 which will be superseded by the Bose Einstein Condensate and Cold Atom Laboratory (BECCAL; Frye et al., 2021) in the near future. The aforementioned experiments do not fulfill the requirements of, e. g., volume or power consumption of a satellite platform which is typically used for a gravimetry mission. The Horizon Europe funded CARIOQA Pathfinder Mission Preparation project[1] aims to build a quantum accelerometer engineering model. This project has been supplemented in 2024 by the CARIOQA Phase A study[2] in order to deploy a quantum space gravimetry pathfinder mission (Lévèque et al., 2022) before the year 2030.

1.3. Quantum accelerometers on-board future gravimetry missions

According to Eq. (1), the sensitivity of the CAI can be increased by increasing the interrogation time T. In terrestrial applications, T is limited by the length of the free fall distance of the atoms, e. g.up to 300 ms for a transportable (Freier et al., 2016) and up to a couple of seconds for stationary instruments (Asenbaum et al., 2020; Schilling et al., 2020). As atoms and satellites in space are in free fall, longer separation times T are possible. There, a quantum accelerometer would allow for monitoring the deviation from the free fall trajectory resulting from non-gravitational accelerations acting on the satellite. A limiting factor on the maximum achievable interrogation time is then the residual thermal expansion of the atomic cloud.

The potential sensitivity gain allowed by the increase of the interrogation time up to a few seconds would make CAI accelerometers a competitive technology for future satellite gravity missions (Abrykosov et al., 2019). They indeed provide absolute measurements and high long-term stability. While this would also be highly beneficial in a hybridized configuration with classical sensors (e. g.a relative electrostatic accelerometer (E-ACC)), the present study focuses on the performance of the CAI itself.

HosseiniArani et al. (2022) have shown a Kalman-filter-based hybridization strategy of an electrostatic accelerometer with the characteristics of the GRACE-FO mission with a CAI accelerometer based on state-of-the-art technology to create a hybrid accelerometer on-board a future satellite gravity mission. HosseiniArani et al. (2022) assumes an achievable sensitivity of 1×10^{-10} m/s^2/$\sqrt{\text{Hz}}$ based on an improvement of two order of magnitudes from ground applications in gravimetry (Merlet et al., 2021) thanks to an extension of the interrogation time to several seconds. Additionally, the objective of current technology developments is also at the 10^{-10} m/s^2/$\sqrt{\text{Hz}}$ level, e. g.in the Horizon Europe funded CARIOQA-PMP project (Lévèque et al., 2022) preparing a demonstration of a quantum accelerometer in space.

[1] https://doi.org/10.3030/101081775
[2] https://cordis.europa.eu/project/id/101135075

In this paper, we will investigate the current and future advances in atom interferometry and study their impacts on the performance of quantum sensors on-board future satellite gravity missions. In Section 2, we describe our modeling environment and the theoretical background of the cold atom interferometer model. In Section 3, we discuss the effect of various parameters on the atom interferometer sensitivity. Finally, in Section 4 we evaluate different atom interferometer configurations for satellite applications.

2. Modeling

2.1. Orbit model

We consider a GRACE-like satellite pair in a circular polar orbit around the Earth with an altitude of 480 km. The simulation is implemented in the MATLAB/Simulink-based eXtended High-Performance satellite dynamics Simulator (XHPS; Wöske et al., 2019) developed by ZARM/DLR. XHPS calculates the orbits of a GRACE-FO mission scenario under consideration of the Earth's gravity field (EGM 2008 up to d/o 90; Pavlis et al., 2012), non-gravitational forces (atmospheric drag, solar radiation pressure, Earth albedo and thermal radiation pressure) and the GRACE-FO satellite geometry. To consider the effect of non-gravitational forces on the spacecraft, we use a detailed surface model of the satellite body included in XHPS.

2.2. CAI accelerometer signal model

The highest contribution to the signal of the CAI accelerometer arises from the non-gravitational accelerations. The phase shift generated by a constant acceleration signal would be given by Eq. (1). However, since the non-gravitational acceleration varies during the CAI interrogation time, we use the integrated form of Eq. (1), considering the sensitivity function as described in Knabe et al. (2022). The phase of interferometer Φ_k at the k-thmeasurement is given by

$$\Delta\Phi = 2k_{\text{eff}}\left[\int_{kT_c}^{(k+1)T_c} g_{a,k}a(t)\,dx\right] \tag{2}$$

where $g_{a,k}$ is the sensitivity of the instrument. T_c is the duration of each interferometer measurement cycle, which consists of a preparation time T_p, the interferometer duration $2T$ and a detection time T_d. We neglect here T_d since it lasts only a few tens of ms, but also T_p, despite the typical duration of the order of one second. Therefore, the sampling rate of the quantum sensor would be equal to $1/2Ts^{-1}$.

2.3. Modeling of the rotational effects

In addition to the phase shift caused by the non-gravitational signal, we consider rotational contributions to the interferometer phase, which come from the fact that the satellite rotates about its cross-track (Y-) axis with a rotation rate of ≈1.1 mrad/s to stay in a nadir-pointing orientation. This rotation creates additional phase contributions, which depend on the position of the CAI accelerometer inside the satellite and also the direction of its sensitivity axis.

The largest contribution of this rotation to the phase shift of the atom interferometer arises from the Coriolis acceleration induced by the atomic velocity in the radial direction (Lévèque et al., 2021). In addition, there are also Euler and centrifugal contributions.

As discussed in Section 1.3, in this study we consider the CAI accelerometer to be used in combination with E-ACC. Since both instruments cannot be co-located, placing the E-ACC at the center of mass of the satellite requires a displacement of the position of the atoms with respect to the center of mass, resulting in a gravity gradient and a gravitational pull of the spacecraft's mass on the atoms.

The positioning of the CAI accelerometer within the satellite can play an important role in the achievable sensitivity. Fig. 2 compares the different possible positions for the CAI accelerometer inside the satellite. Here, the E-ACC is assumed to be at the center of mass of the satellite while the CAI is shifted from it. The CAI accelerometer is placed either in front of the E-ACC on the along-track axis, on top of the E-ACC on the radial axis or next to the E-ACC on the cross-track axis of the satellite.

In a configuration similar to Fig. 2-a, the centrifugal and Coriolis accelerations are in the direction of the sensitivity axis, but the Euler acceleration is perpendicular and, therefore, is not sensed by the CAI accelerometer. In a configuration similar to Fig. 2-b, the Coriolis and Euler accelerations are aligned with the CAI accelerometer sensitivity axis, and the centrifugal acceleration is perpendicular to it. In configuration b, because of the displacement in the radial direction, the Earth's gravity gradient imposes an additional error on the CAI accelerometer. In the third configuration (Fig. 2-c), the centrifugal and Coriolis accelerations are aligned with the sensitivity axis. However, the centrifugal acceleration has a considerably smaller value (close to zero) because the lever arm is now reduced to a distance close to the movement of the center of mass. As a consequence, the latest positioning shows considerable advantages compared to the other two possible cases.

This phase shift due to the satellite rotation can be calculated from the following equations (Beaufils et al., 2023):

$$\begin{aligned}\Delta\Phi = 2k_{\text{eff}}T^2[a_x + 2v_{z0}(\Omega_y + \Omega_M) - x_0\Omega_y^2 \\ +(x_0 - x_M)(\Omega_M{}^2 + (\Omega_M - \Omega_I)^2)]\end{aligned} \tag{3}$$

where x_0 is the initial distance of atoms to the satellite center of mass, x_M is the distance of the center of rotation of the mirror to the satellite center of mass, Ω_y is the angular velocity of the satellite around the cross-track axis with respect to the inertial frame, Ω_M and Ω_I are the angular velocities of the mirror and incoming laser beam, with

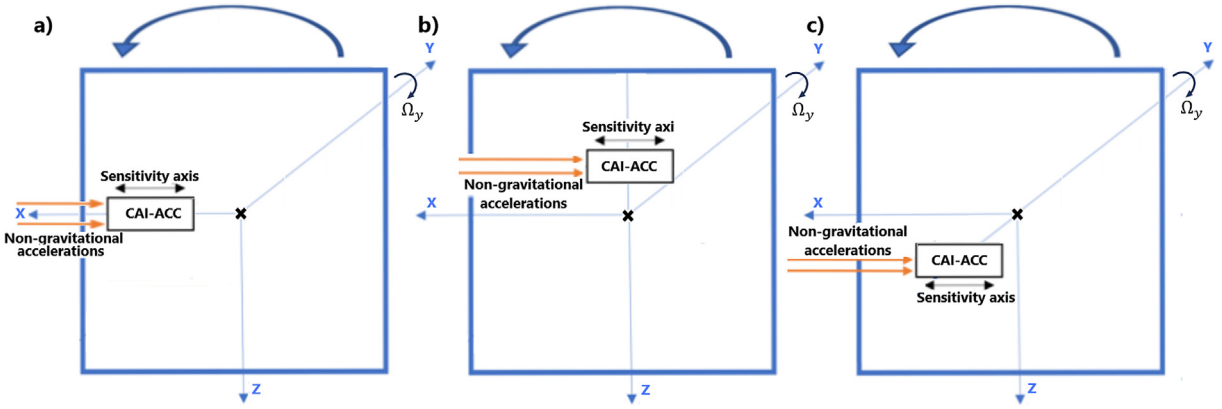

Fig. 2. Positioning of the CAI accelerometer inside the satellite frame with the E-ACC at the center of mass; a: The CAI accelerometer is placed on the along-track axis of the satellite, offset from the center of mass; b: The CAI accelerometer is placed on the radial axis of the satellite, offset from the center of mass; c: CAI accelerometer is placed on the cross-track axis of the satellite, offset from the center of mass; In all positions, the sensitivity axis of the CAI accelerometer is parallel to the along-track axis of the satellite. Only the along-track component of the non-gravitational accelerations, which is parallel to the sensitivity axis of the CAI accelerometer, is displayed.

respect to the satellite body-fixed frame, and v_{z0} is the initial velocity of atoms in the radial direction and in the satellite frame.

The rotational phase shift could add extremely large errors to the measurements of the quantum sensor if they are not properly compensated. Different approaches have been proposed to compensate for the rotation effect. The impact of the main rotation due to the orbital frequency can be compensated by counter-rotating the Raman wave vector with a fixed rate; (see e. g., Trimeche et al., 2019, for a nadir pointing gradiometer). This approach would not compensate for the residual rotation error.

In another approach, a high-performance onboard gyroscope can be used to measure the satellite rotation at each instant in time and cancel its contribution to the phase shift by an active Raman mirror rotating against the rotation rate of the satellite (Lan et al., 2012; Migliaccio et al., 2019). In this scenario, the incoming laser is assumed to be fixed in the body frame of the satellite and has a rotation rate identical to that of the satellite, therefore

$$\begin{aligned} \Omega_M &= -\Omega_y \quad \text{and} \\ \Omega_I &= 0. \end{aligned} \tag{4}$$

We also assume that the center of rotation of the mirror is the same as the center of mass of the satellite ($x_M = 0$). With these assumptions, Eq. (3) becomes

$$\Delta\Phi = 2k_{\text{eff}}T^2[a_x + x_0\Omega_y^2]. \tag{5}$$

The term $x_0\Omega_y^2$ would be the remaining term which could induce a bias in the measurements of the CAI accelerometer. We need to stress that apart from the remaining term, the phase shift contains residual terms related to the difference between the rotation rate of the mirror and the satellite rotation rate due to imperfect calibration and noise in the rotation sensors and actuators. Furthermore, there are smaller rotation components around the other axes in addition to the main rotation of the satellite around the cross-track axis. These residual terms would also result in additional phase shift components. For a comprehensive and accurate modeling, these residual terms are also accounted for in this study.

The third approach considered in this study is the counter-rotation of the entire quantum sensor. This approach would be technically challenging. Nevertheless, we investigated it and compared the performance of the quantum sensor when different rotation compensation techniques were applied. Note that in this approach, the quantum sensor would be counter-rotated against the satellite, which would keep rotating around its cross-track axis to keep the nadir-looking orientation.The assumption for this approach is:

$$\Omega_M = \Omega_I = -\Omega_y. \tag{6}$$

With this assumption, Eq. (3) will become

$$\Delta\Phi = 2k_{\text{eff}}T^2[a_x - x_M\Omega_M^2], \tag{7}$$

leading to a centrifugal bias, which vanishes if the center of rotation of the Raman mirror coincides with the satellite center of mass ($x_M = 0$). Note that this very center of rotation can differ from the mirror center of mass, so that even if the mirror is not positioned at the satellite center of mass, its rotation center can. One should stress that, similar to the previous case, the phase shift contains residual terms related to the difference between the rotation rate of the mirror andthat of the satellite, due to imperfect calibration and noise in the rotation sensors and actuators. However, these residual terms are negligible.

2.4. CAI accelerometer noise model

In this study, we consider a full noise model that includes all the major noise sources that affect the measured phase shift. In Section 2.3, we discussed the environmental noises that impact the CAI accelerometer

measurements. Below, we discuss the quantum and instrumental errors that are modeled in this study:

Frequency noise of the master Raman laser. While the noise in the phase difference between the lasers does not impact the sensitivity of the measurement in the double diffraction mode (Lévèque et al., 2009), the frequency noise of the master Raman laser does (Le Gouët et al., 2007). We assume here a white noise for the master Raman laser frequencywith the variance of $\sigma_\phi^2(LN)$. This noise contribution then scales inversely to the duration of the Raman pulses and proportionally to the distance to the mirror (Le Gouët et al., 2007).

Wavefront aberrations noise. Wavefront aberrations induce noise in the interferometer phase (Louchet-Chauvet et al., 2011) that originates from the motion of the atoms in the distorted phase profile of the Raman laser beams. Wavefront aberrations are decomposed onto the basis of Zernike polynomials ($Z_n^m(\rho\theta)$), with $\rho = r/R$ the radius normalized by the reference radius R. We assume R to be the radius of our retro-reflecting mirror ($R = R_m$). Table 1 gives the expression of the lowest polynomials, the related aberration, and the corresponding interferometer phase shifts. The phase shifts are averaged over the velocity distribution for initial positions x_0 and y_0 of the atomic cloud. Here, the initial size of the cloud is neglected. Since the (Raman differential) wavefront is given by

$$\sigma(\rho,\theta) = \Sigma A_n^m Z_n^m(\rho\theta), \tag{8}$$

the aberration bias is the sum of the interferometer phase shift terms in Table 1, weighted by the coefficients A_n^m, where t_1 is the delay of the first Raman pulse with respect to the release time of the atoms, and σ_v is the initial velocity dispersion of the atomic cloud.

Generally speaking, the aberration bias gets lower with a flatter Raman mirror, with a lower atomic temperature, and with a shorter interrogation time. It fluctuates with the initial position and velocity of the atomic source with respect to the laser beam, adding noise to the measurement.

Detection noise. Detection noise has two components: Quantum projection noise (QPN), which is the quantum standard limit in quantum inertial sensors and clocks, and technical noise (TN), for instance, due to electronic noise on the measurement of the number of atoms. Both QPN and TN generally get lower with a higher number of atoms, but TN also has a constant term,independent of the number of atoms. So, in the end, one has

$$\sigma_P^2(QPN) = \frac{P(1-P)}{N}, \tag{9}$$

$$\sigma_P^2(TN) = \frac{P^2\sigma_{N_2}^2 + (1-P)^2\sigma_{N_1}^2}{N^2} + \sigma_P^2(\infty), \tag{10}$$

$$\sigma_P^2(DET) = \sigma_P^2(QPN) + \sigma_P^2(TN). \tag{11}$$

where, $\sigma_P^2(QPN)$ and $\sigma_P^2(TN)$ and $\sigma_P^2(DET)$ are the variances of the transition probability due to the QPN, TN and total detection noise respectively, σ_{N_i} is the electronic noise on the measurement of the number of atoms in the i-th port and $\sigma_P^2(\infty)$ is a contribution independent of the number of atoms. The latest is the dominating factor at a very large number of atoms. It is related to frequency and intensity noise on the detection laser and to normalisation noise.

Contrast loss. Loss of contrast in the atom interferometer results in a loss of sensitivity in the measurement of the phase shift. It has two main sources. The first is the inhomogeneity of the laser intensity experienced by the atoms. Since the atomic cloud has a finite size and residual expansion, laser intensity inhomogeneity across the atomic cloud leads to coupling inhomogeneities, which induce losses in the number of atoms and in contrast. The second source is Coriolis acceleration, which leads to inhomogeneous dephasing due to the finite temperature of the atomic cloud. Averaging the Coriolis acceleration over the velocity distribution then leads to a loss of contrast.

The loss of contrast due to the laser intensity inhomogeneity gets lower with lower atomic temperatures and shorter interrogation times. It also gets lower with larger laser waists. As for the loss due to Coriolis acceleration, it gets lower with lower angular velocities, shorter interrogation times, and lower temperatures (T_0).For more information about the modeling of the contrast loss, we refer toLan et al. (2012) and Cheng et al. (2014).

Other sources of noise. The sensitivity of the quantum accelerometer can be degraded by vibration noise directly due to fast fluctuations of the non-gravitational accelerations acting on the satellite body, e.g., solar and planetary radiation pressure and atmospheric drag, or more indi-

Table 1
Zernike polynomials and the corresponding interferometer phase-shifts.

Zernike polynomial (Z_n^m)	related aberrations	Phase shift ($\Delta\Phi$)
Piston (Z_0^0)	1	0
Tilt x (Z_1^1)	$\rho\sin\theta$	0
Tilt y (Z_1^{-1})	$\rho\cos\theta$	0
Focus (Z_2^0)	$2\rho^2 - 1$	$8T^2\sigma_v^2/R^2$
Astigmatism 0°(Z_2^2)	$\rho^2\sin 2\theta$	0
Astigmatism 45°(Z_2^{-2})	$\rho^2\cos 2\theta$	0
Coma X (Z_3^{-1})	$\rho sin\theta(3\rho^2 - 2)$	$24T^2x_0\sigma_v^2/R^3$
Coma Y (Z_3^1)	$\rho cos\theta(3\rho^2 - 2)$	$24T^2y_0\sigma_v^2/R^3$
Spherical aberration (Z_4^0)	$6\rho^4 - 6\rho^2 + 1$	$24T^2\sigma_v^2 f(R,x_0,y_0,t_1,T,\sigma_v)/R^4$*

* $f(R,x_0,y_0,t_1,T,\sigma_v) = (x_0^2 + y_0^2 + \sigma_v^2(6t_1^2 + 12t_1T + 7T^2)) - R^2)$

rectly due to excitation of structural modes by fast-changing accelerations either internal or external to the satellite. One of the main sources of structural vibrations is often mechanical processes originating in the satellite interior, e.g., reaction wheels, mass trim mechanisms and propellant sloshing. For GRACE-like satellites, because of the absence of any rotating solar panels and employing optimized fuel tanks, we consider such vibrations to be negligible. Moreover, internal structural vibrations are typically very short, vanishing after a few seconds(Flury et al., 2008). Thanks to the high 10 Hz sampling rate of the electrostatic accelerometers onboard GRACE and GRACE-FO missions, such short effects are well observed.

Transition Probability. The measured transition probability at the $k-th$ measurement cycle is given by

$$P_k = [1/2 \times C_{inho}(1 - C_{cor} \times \cos(\Delta\Phi_k + \delta\phi_k)] + \delta_{P_k} \quad (12)$$

with C_{inho} and C_{cor}, being the contrast losses, and $\Delta\Phi_k$, the deterministic interferometer phase shift one can calculate for the $k-th$ cycle of the non-gravitational accelerations acting on the satellite during the CAI interrogation time. δ_{P_k} is a random noise contribution with the variance of the detection noise $\sigma_p^2(DET)$ presented earlier in this section. $\delta\phi_k$ is a random phase noise as

$$\delta\phi_k = \delta\phi_k(LN) + \delta\phi_k(WA) + \delta\phi_k(rot) \quad (13)$$

where $\delta\phi_k(LN)$ is a random phase noise due to laser frequency fluctuations, with the variance of the frequency noise of the master Raman laser $\sigma_\phi^2(LN), \delta\phi_k(WA)$ is the wavefront aberration phase noise, and $\delta\phi_k(rot)$ is a contribution related to rotations.

3. Sensitivity analysis

3.1. Sensitivity to the positioning and rotation

It will be shown later that the rotational phase shift can wash out the contrast if not properly compensated (see Fig. 3). In Section 2.3, we discussed three possible approaches to physically compensate for the rotation of the satellite. In this section, we discuss the impact of the rotation compensation method used together with the effects of the positioning of the CAI accelerometer inside the satellite frame, on the measurement noise.

First, we assume that the CAI accelerometer is positioned in front of the E-ACC on the along-track axis of the satellite. This is a default position, actually considered in some studies (Abrykosov et al., 2019; Zahzam et al., 2022). We then study the three possible methods for the compensation of the rotation when the CAI accelerometer is placed in this position. We also try another possible configuration, in which we consider the CAI to be positioned on the cross-track axis of the satellite. There, the sensitivity axis would still be parallel to the along-track axis (see Fig. 2). Then, we investigate the impact of different rotation compensation methods in this configuration. In this study, we do not consider a configuration similar to Fig. 2-b since it shows the worse result coming mostly due to the impact of the radial gravity gradient.

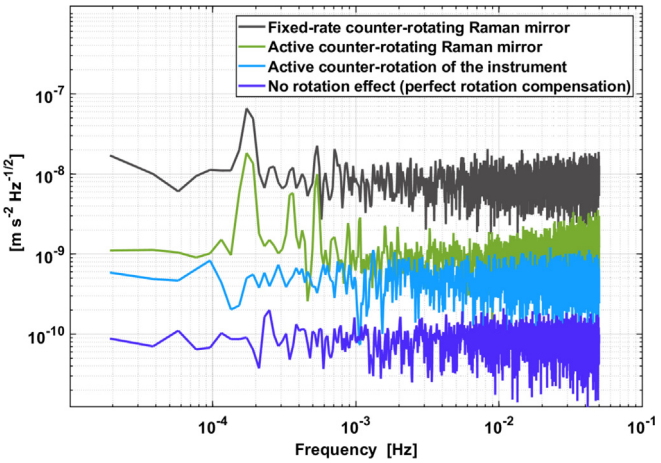

Fig. 3. Amplitude spectral density for the CAI accelerometer measurement noise in the state-of-the-art scenario as defined in Section 4.1; Different colours represent different assumptions on the rotation compensation method of the CAI accelerometer. All curves are produced with the assumption that the CAI accelerometer is placed on the along-track axis of the satellite and in front of the E-ACC. In all scenarios, the sensitivity axis of the CAI accelerometer is assumed to be parallel with the along-track axis.

In Section 2.3, we discussed three possible approaches to compensate for the rotation effect. In the case of counter-rotation of the Raman mirror with a fixed rate, the uncompensated part of the rotation would be the difference between the true turn rate of the satellite and the fixed rotation rate of the mirror. By contrast, when an active counter-rotation using the gyroscope's data is assumed, the uncompensated rotation rate would be equal to the noise of the gyroscope (see Table 2). It is worth mentioning that, in reality, the steering actuator, the loop design, potential transients and delays would also contribute to uncompensated rotation error. However, we consider them negligible compared to the noise of the gyroscope.

Our simulations results indicate that an error in the atomic cloud's initial positioning, combined with the uncompensated rotation rate, could result in an additional uncompensated centrifugal acceleration, causing noise in the measurements. This additional random noise would be one of the largest noise sources, especially in the case of rotation compensation using counter-rotating Raman mirrors.

Fig. 3 compares the impact of different assumptions for the rotation compensation for a state-of-the-art CAI accelerometer, indicating the importance of a proper rotation compensation technique. For the sake of simplicity, we will only consider the dominant rotation around the cross-track axis in the following discussion. However, the rotation rates around the other two axes, although much smaller, also result in additional terms for the Coriolis, centrifugal, and Euler accelerations and, thus, additional

Table 2
Assumptions for the CAI accelerometer on-board gravity missions.

Scenario	CAI accelerometer based on state-of-the-art technology	Near-future CAI accelerometer in space	Far-future CAI accelerometer in space
Expected time	expected for launch in 5 years	next 10–15 years	next 20–25 years
Laser Waist	6 mm	20 mm	40 mm
Atomic temperature (T_0)	100×10^{-12} K	10×10^{-12} K	1×10^{-12} K
Temperature stability	4×10^{-12} K	1×10^{-12} K	0.5×10^{-12} K
Number of atoms	5×10^5	1×10^6	1×10^7 or 1×10^6 and 10 db squeezing
Technical noise [a] constant term ($\sigma_p(\infty)$)	1×10^{-4}	1×10^{-4}	1×10^{-5}
Rotation compensation	Counter-rotating mirror	Counter-rotating mirror or counter-rotating CAI sensor	Counter-rotating mirror or counter-rotating CAI sensor
Initial positioning of the atomic cloud	1×10^{-4} m	1×10^{-4} to 1×10^{-5} m[b]	1×10^{-5} to 1×10^{-6} m[c]
Transversal velocity of the atomic cloud	100×10^{-6} m s^{-1}	20×10^{-6} m s^{-1}	5×10^{-6} m s^{-1}
Noise of gyro (white noise)	6.6×10^{-7} rad s^{-1}	6.6×10^{-8} rad s^{-1}	6.6×10^{-9} rad s^{-1}
Noise of E-ACC[d] (at higher frequencies)	1×10^{-10} m/s^2 (1×10^{-3} to 10^{-1} Hz)	1×10^{-11} m/s^2 (1×10^{-3} to 10^{-1} Hz)	1×10^{-12} m/s^2 (1×10^{-3} to 10^{-1} Hz)
Atomic flight time ($2T$)	5 to 10 s	10 s	10 to 20 s

[a] Technical noise is one of the contributions of the detection noise. For more information we refer to Section 2.4.
[b] In case of the counter-rotation of the whole CAI sensor, the accuracy of 1×10^{-4} m would be enough; otherwise, we would need a positioning accuracy of 1×10^{-5} m.
[c] In case of the counter-rotation of the whole CAI sensor, the accuracy of 1×10^{-5} m would be enough; otherwise, we would need a positioning accuracy of 1×10^{-6} m.
[d] An E-ACC usually performs best in a frequency range higher than 10^{-3} *Hz*, while at lower frequencies, the measurements suffer from large noise.

phase shifts. These additional error terms will be fully considered in the modeling of the CAI accelerometer noise.

3.2. Sensitivity to the atomic temperatures

The temperature of the atoms plays an important role in the performance of the CAI accelerometer measurements. Fig. 4 shows the contrast loss due to the Coriolis effect as a function of the rotation rate, for different temperatures and for an interferometer duration of $2T = 10$ s. For temperatures in the nK range, uncompensated rotations of the order of a few μrad/s would lead to a significant loss of contrast. Reducing the temperature further down, into to the pK, mitigates this effect.

Fig. 5 illustrates the impact of laser intensity inhomogeneity by displaying the evolution of the contrast with laser waist for different temperatures. One can notice that

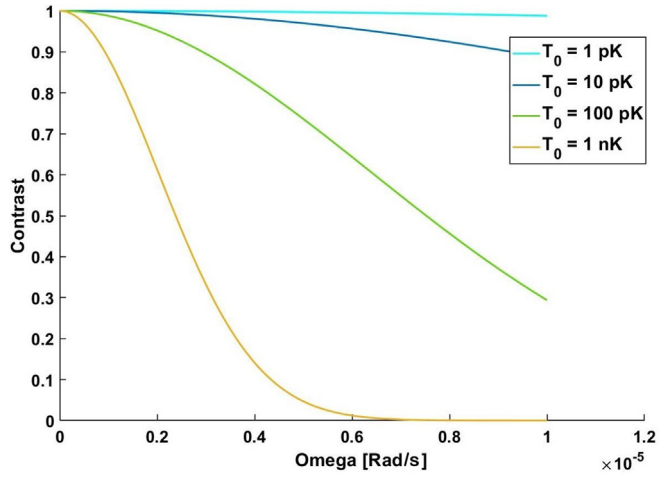

Fig. 4. Contrast loss due to the Coriolis effect as a function of the uncompensated rotation rate of the satellite; Different colours represent different atomic temperatures.

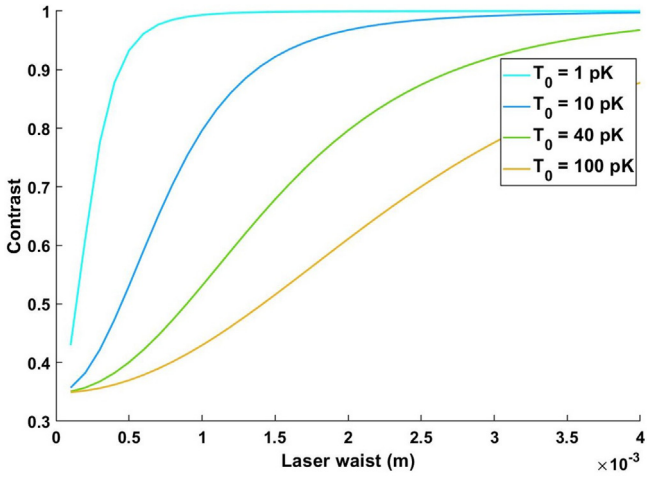

Fig. 5. Contrast loss due to laser intensity inhomogeneity of an atom interferometer as a function of laser waist. Different colours represent different atomic temperatures.

increasing the laser waist is an efficient way to reduce contrast loss.

3.3. Sensitivity to the interrogation time

The interrogation time of the CAI accelerometer is a key parameter in the search for its optimal performance. On one hand, based on Eq. (1), one expects a larger scale factor, and thus a higher measurement sensitivity. On the other hand, some components of the instrumental noise and errors, e. g., wavefront aberration and loss of contrast, get larger when increasing the interrogation time. Whether the performance would be better when increasing the interrogation time depends on the assumptions for the instrument parameters, rotation compensation, and satellite orbit. In practice, there will be an optimal interrogation time for each set of assumptions.

3.4. Sensitivity to the number of atoms

Fig. 6 shows the impact of increasing the number of atoms on the different components of the detection noise. One can see that a higher number of atoms can reduce both QPN and TN. With the current number of atoms in the CAI accelerometers based on the state-of-the-art technology (see Table 2), the total detection noise is around 1×10^{-11} m/s^2/$\sqrt{\text{Hz}}$, which is more than one order lower than the other contributions of noise we have considered in the state-of-the-art scenario (see Figs. 7 and 9). This noise level is also close to the other noise contributions in the near-future scenario. Therefore, we only consider a factor 2 improvement in the number of atoms for the near-future scenario.

Far-future atom interferometry will reach a level of sensitivity better than 1×10^{-11} m/s^2/$\sqrt{\text{Hz}}$, and then, it would be necessary to improve the QPN in order to achieve better sensitivities. Improving the QPN limited sensitivity by increasing the number of atoms could be an option for far-future missions. However, the gain in sensitivity only scales as the square root of the atom number. Pioneering experiments on producing spin-squeezed states of atoms have shown a path toward preparing a state with large spin alignment and noise below the QPN level (Anders et al., 2021; Greve et al., 2022). Therefore, a more suitable strategy for far-future missions could be implementing spin-squeezing techniques to overcome the standard quantum limit (Gross et al., 2010; Hosten et al., 2016).

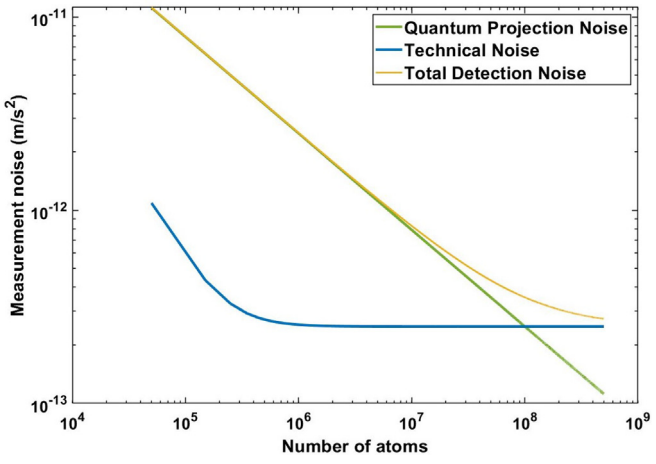

Fig. 6. Sensitivity of the detection noise to the number of atoms; Green: Quantum projection noise; Blue: technical noise; Yellow: total detection noise.

4. In-orbit performance evaluation of CAI Accelerometry

4.1. State-of-the-art atom interferometry in space

We define the state-of-the-art CAI accelerometer in space as the quantum sensor that can be built with the currently available technology. The assumptions used for this scenario are briefly shown in Table 2.

Fig. 7 shows the noise of the state-of-the-art sensor with 10 s interferometry duration in the frequency domain and compares the impact of different assumptions on the positioning and rotation compensation techniques on the noise level. Note that the counter-rotation of the whole quantum sensor would be technically challenging for the state-of-the-art scenario. We only show these plots to compare different rotation compensation methods. It is also important to take into account that in all these approaches, the sensitivity axis of the CAI accelerometer is still parallel to the along-track axis of the satellite and only the position of the CAI accelerometer inside the satellite is changed. The motivation for keeping the sensitivity axis along-track is that the non-gravitational acceleration in the along-track axis is the most critical component for a GRACE-like mission, i.e. the acceleration of the satellite along this direction directly impacts the determination of the gravity field.

The green curve in Fig. 7 shows the case where the CAI accelerometer is placed on the along-track axis of the satellite with a displacement from the center of mass (due to the positioning of E-ACC in the center of mass). According to Eq. (5), not rotating the whole sensor, in this case, would result in a remaining term $x_0\Omega_y^2$ which could cause a measurement bias. This term can, in principle, be mathematically corrected with proper knowledge of the rotational rates and the non-gravitational accelerations. Fig. 8 shows an example of this bias before and after the mathematical correction. Our simulations show that the bias can be removed by two orders of magnitude, providing that a gyro with the accuracy presented in Table 2 exists. For all curves in Fig. 3 and Fig. 7, the mathematical correction is already applied.

Our simulations show that for the atom interferometry in space based on state-of-the-art technology, the optimal interferometer duration ($2T$) would be between 5 to 10 s, with $2T = 5$ s leading to slightly improved results. For near-future atom interferometry, $2T = 10$ s would lead to the best performance. For the far-future scenario, it would be possible to increase the interrogation time even more.

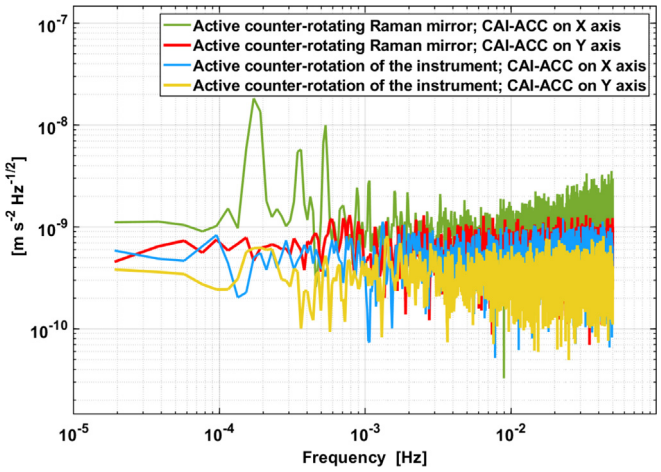

Fig. 7. Amplitude spectral density for the CAI accelerometer measurement noise in the state-of-the-art scenario as defined in Section 4.1. Different colours represent different assumptions on the positioning and rotation compensation method of the CAI accelerometer. In all scenarios, the sensitivity axis of the CAI accelerometer is assumed to be parallel with the along-track axis.

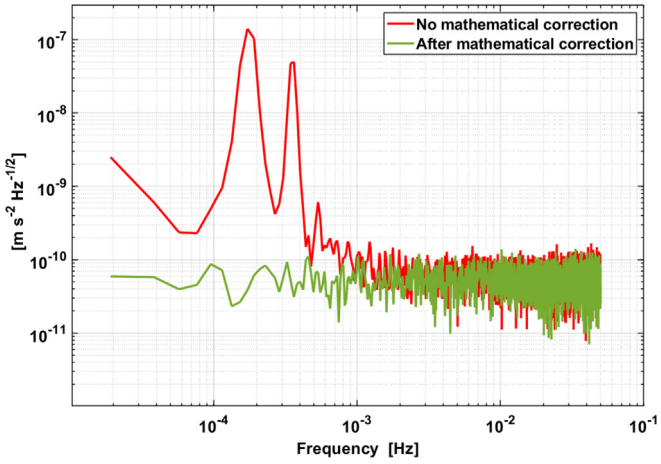

Fig. 8. Amplitude spectral density for the CAI accelerometer measurement noise before and after the mathematical compensations of the low-frequency bias. The CAI accelerometer is positioned on the long-track axis of the satellite and in front of the E-ACC. The largest bias amplitude shows up at the orbital frequency.

We demonstrate that an interferometer duration of $(2T)$ of 20 s leads to considerably improved results.

Improving quantum accelerometers beyond their current limits is a current challenge being tackled by a number of research groups worldwide. This gives way to the following prospective scenarios for future gravity missions with on-board quantum accelerometers. We first define a "near-future" scenario with improvements expected in the next 10–15 years. We then define a "far-future" scenario for expected improvements in the next 20–25 years.

4.2. Future advances in atom interferometry in space

Intense research efforts are being made on scientific and engineering aspects to advance atom interferometry. All those aspects are important for atom interferometry. However, the question arises which aspects should be improved first or later to achieve maximum efficiency at each future period. The answer to this question would allow establishing a roadmap for future developments of quantum sensors for satellite gravity missions by improving the most impactful parameters.

QPN acts as a natural noise limit for atom interferometry. For the near-future scenario, our strategy is to try to reduce other error sources down to the QPN level and find a path for future advances in atom interferometry, which optimizes the efforts. We would need a roadmap that both considers the impact on the performance of the CAI sensor and the technical limits. Table 2 is created using this strategy and shows the assumptions for different mission scenarios.

As shown in Fig. 9, the state-of-the-art scenario is limited by the contrast loss due to the laser intensity inhomogeneity and wavefront aberration noise. It is also considerably limited by the Coriolis and centrifugal accelerations caused by the uncompensated part of the rotation rate. QPN is a negligible noise source in this scenario. Going to the near-future scenario on the same figure, we notice that by the improvements suggested in Table 2, all the noise sources have reduced to the level of QPN.

Fig. 3 shows the impact of different rotation compensation methods for the CAI accelerometer based on state-of-the-art technology. Without rotation compensation, the loss of contrast would limit the maximum interrogation time to a few hundred milliseconds only, so counter-rotation of the mirror is mandatory for performing acceleration measurements. With a fixed-rate counter-rotating Raman mirror, though the contrast would remain larger than 50% at all times, the acceleration noise would remain limited by fluctuations of the residual Coriolis and centrifugal accelerations to the $10^{-8}\mathrm{m.s}^{-2}/\mathrm{Hz}^{1/2}$ level.

Better performances are met when actively compensating the rotations. When counter-rotating the mirror actively with the quantum accelerometer placed in front of the E-ACC on the along-track axis of the satellite, there remains a bias in the measurements though, fluctuating at the orbital frequency, related to the term discussed above in Eq. (5). While this term could, in principle, be mathematically corrected for with proper knowledge of the rotational rates and the non-gravitational accelerations (see Fig. 8), it could also be eliminated by either counter-rotating the whole CAI sensor inside the satellite (see the blue curve in Fig. 7), which would be technically very challenging, or more simply by positioning the CAI sensor on the cross-track axis of the satellite (the red curve in Fig. 7). Note that for all curves, the sensitivity axis of the CAI accelerometer is always assumed to be parallel with the along-track axis, and only the sensor's position is changed between the different scenarios.

While relatively small laser waists, in the range of 1.5mm to 6mm, can be sufficient for ground-based measurements

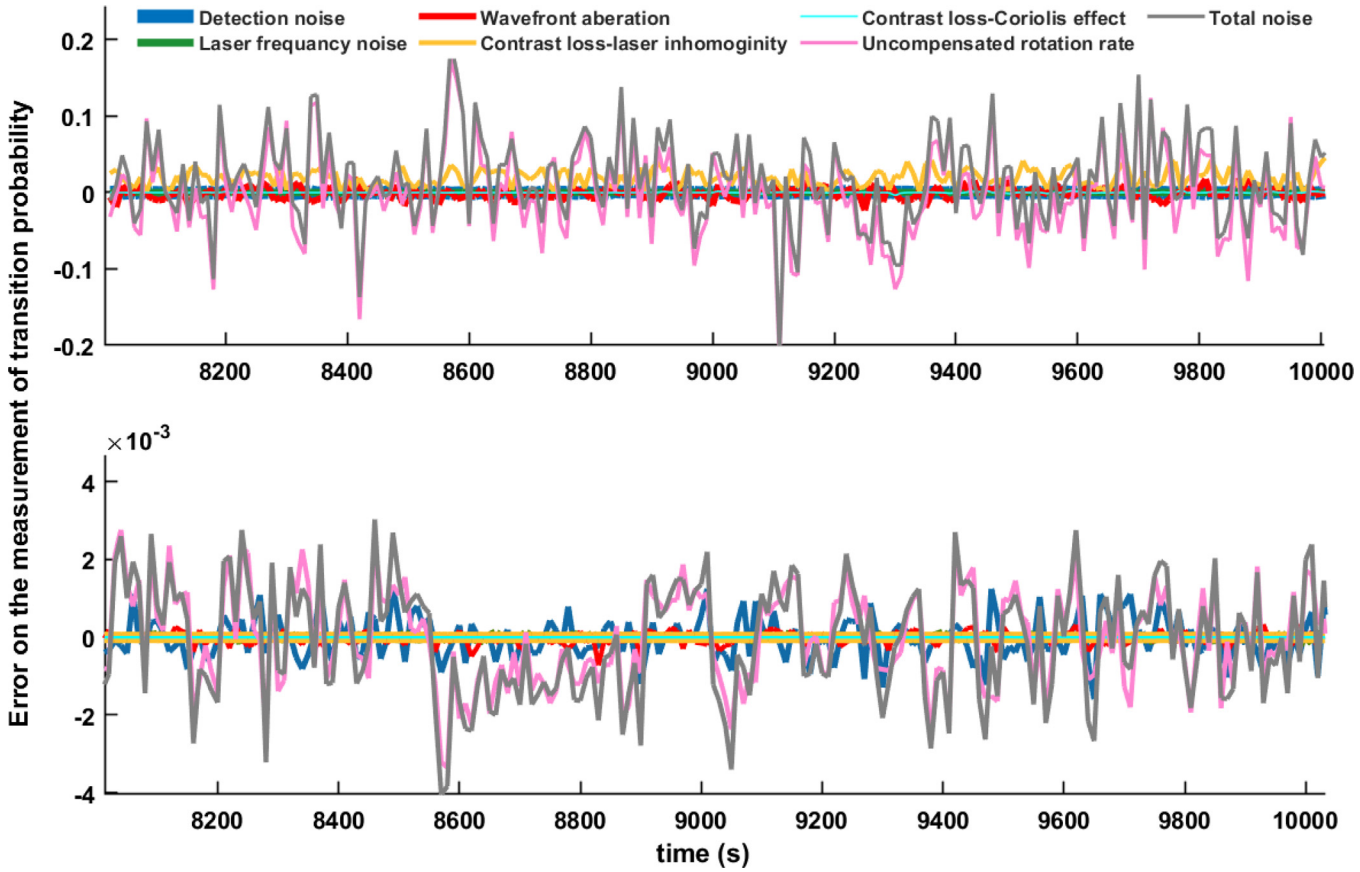

Fig. 9. Simulation of the noise time series for a CAI accelerometer based on state-of-the-art technology (top plot), and for a near-future CAI accelerometer (bottom plot) for 1000 s. To compare the impact of different noise sources on the total noise, the components of the noise are plotted separately. To avoid the impact of initial fluctuations on the CAI measurements, we start the simulations of the CAI accelerometer after the stabilization of the satellite angular velocity (here, 8000 s after the start of the orbit propagation).

(Chiow et al., 2011; Merlet et al., 2014), which motivated our choice of 6mm for the scenario based on state-of-the-art technology, we consider here a relatively large laser waist of 20mm for the near-future scenario. Reaching a Rabi frequency of 16kHz at a Raman detuning of 3.4GHz, which optimizes the performance of the double-diffraction interferometer, demands laser powers of about 100mW and 360mW per beam, which matches with the typical powers achievable with current compact laser systems. Therefore, we consider this laser waist for near-future mission scenario. The required power scaling with the laser waist to the square, a waist of 40mm would lead to powers of about 400mW and 1.44W, which are more demanding in terms of technology. We have thus considered these laser parameters for the far-future mission scenario.

As discussed, having an active rotation compensation method (e.g., active counter-rotating mirrors) is necessary in order to achieve a level of sensitivity close to the QPN level. For this, accurate gyros are needed to provide information about the satellite angular rate, cf. Table 2. For the state-of-the-art mission, we assume gyros similar to the gyro of GRACE-FO satellites (see Table 2). However, for the near-future and far-future mission scenarios, we assume gyros with noise performances of one and two orders of magnitude better than the state-of-the-art ones. As discussed in Section 1, having in view a hybrid accelerometer configuration, we consider the integration of an electrostatic accelerometer in parallel with the CAI accelerometer. To fully benefit from such a hybrid configuration, the sensitivity floor of the E-ACC at higher frequencies should be at the same level as the CAI accelerometer. Therefore, for the near-future and far-future mission scenarios, we assume an E-ACC one order and two orders of magnitude more sensitive than the current state-of-the-art E-ACCs.

The lowest atomic temperature demonstrated by now is around 40pK, achieved with the Delta kick method (Deppner et al., 2021; Xie et al., 2022). We thus assume this temperature for the state-of-the-art scenario. Based on the ongoing advances in this field, an atomic temperature of 10pK is considered for near-future missions and an atomic temperature of 1pK for far-future missions.

Based on the assumptions we consider for the near-future mission scenario, all the instrumental and environmental noise components reach a noise level close to QPN. Beyond this, the only way to improve the CAI accelerometer would be to reduce the QPN by increasing

the number of atoms or implementing quantum metrology protocols to bring down the detection noise below the standard quantum limit, implementing quantum correlations in the atomic source via spin-squeezing for instance. Therefore, for the far-future scenario, we consider an order of magnitude improvement in the detection noise variance, which we believe is within reach.

We finally perform several simulation studies based on the modeling explained in Section 2 and based on the different sets of assumptions that are shown in Table 2. Figs. 10 and 11 show the estimated measurement noise of the near-future and far-future quantum accelerometers with different assumptions for the sensor. While the difference between rotation compensation using counter-rotating Raman mirrors and using the counter-rotation of the whole quantum sensor is small for state-of-the-art missions (see Fig. 7), these techniques could result in a difference of about a factor of 3 or 4 in the noise level of the near and far future scenarios (see Fig. 10 and Fig. 11). A large part of this difference is a direct result of an error in the initial positioning of the atomic cloud, which causes a large uncompensated centrifugal acceleration for the case we only rotate the Raman mirror (see Eq. (5)).

In the near future, it would be enough if the Raman mirror is rotated against the satellite's main rotation around the cross-track axis. However, we found that for the far-future scenario, to compensate for the rotation to the required level, it would be necessary to also rotate the Raman mirror against the smaller rotation rate of the satellite around the radial axis.

While the optimal interferometry duration for the near-future scenario is around 10 s, for the far-future scenario, increasing the interferometry duration beyond 10 s would be possible. The optimal interferometry duration for this scenario is around 20 s, which results in a noise level lower than 1×10^{-12} m/s^2/$\sqrt{\text{Hz}}$ in case of the counter-rotation of the whole sensor. For the case of counter-rotation of the Raman mirror, increasing the interferometry duration beyond 10 s would not improve the solution.

Fig. 12 compares the amplitude spectral density of the CAI accelerometer measurement noise for the different scenarios in one plot considering the use of an active counter-rotating Raman mirror and the positioning of the CAI accelerometer on the cross-track axis of the satellite (see Fig. 2).

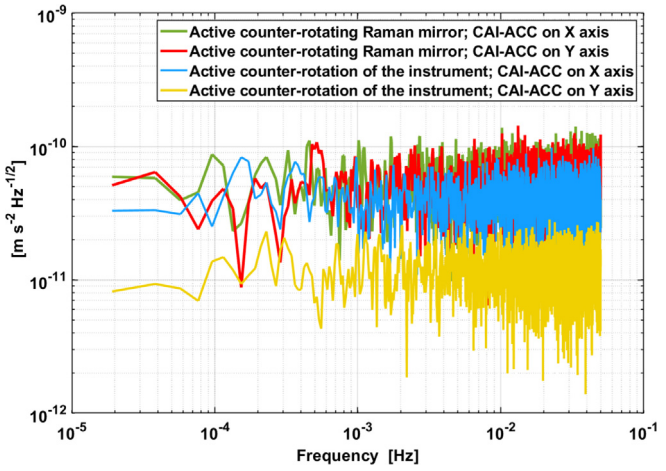

Fig. 10. Amplitude spectral density for the CAI accelerometer measurement noise in the near-future scenario. Different colours represent different assumptions on the positioning and the rotation compensation method of the sensor.

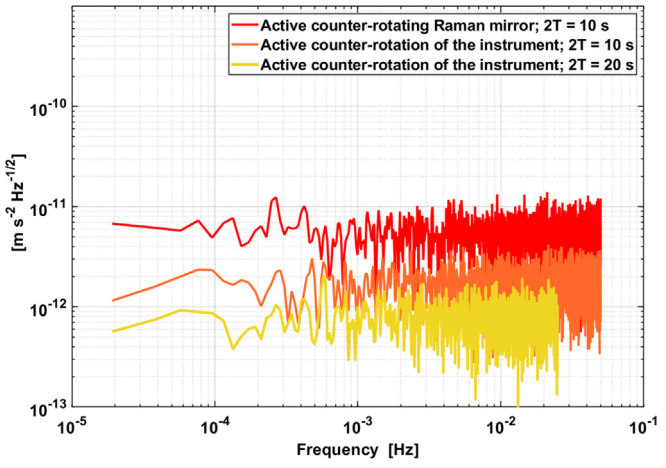

Fig. 11. Amplitude spectral density for the CAI accelerometer measurement noise in the far-future scenario; Different colours represent different assumptions on the positioning and rotation compensation method of the CAI accelerometer.

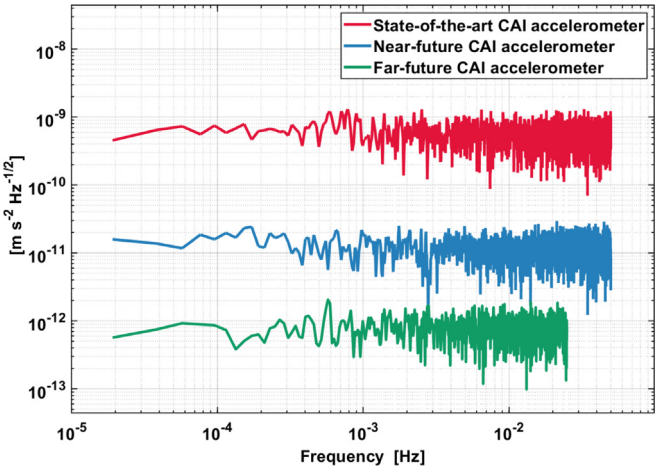

Fig. 12. Comparison of the amplitude spectral densities for the CAI accelerometer measurement noises in the state-of-the-art, near future (in 10–15 years) and far-future (in 20–25 years) scenarios; For all scenarios active counter-rotating Raman mirrors are assumed and the CAI accelerometer is positioned on the cross-track axis of the satellite.

4.3. Ultra-sensitive atom interferometry in space

Since future space missions would require even more sensitive absolute accelerometers, we discuss in this section the possibility of pushing further down the sensitivity of quantum accelerometers. As discussed in Section 2.2, the sensitivity of a quantum accelerometer increases with a longer interrogation time, and being in space would allow to benefit from this. State-of-the-art atom interferometry, still under development for space applications, is considering an interrogation time in the order of a couple of seconds (Lévèque et al., 2022; Beaufils et al., 2023; Zahzam et al., 2022). In this study, we have considered the state-of-the-art and near-future quantum accelerometers to have interferometry duration between $2T = 5$ to 10 s and for the far-future quantum sensors, we show that we can reach an interferometry duration of $2T = 20$ s. But, with the advances that are expected in this field, even longer interrogation times will be possible.

To have a quantum accelerometer with longer interrogation times, one would need to consider that apart from getting larger signals, some components of the error (e.g. contrast loss) would also get larger magnitudes. Really benefiting from longer free flight times will demand to carefully limit these error sources. Fig. 13 displays the loss of contrast as a function of the uncompensated part of the rotation for different interrogation times, showing that the drop in contrast gets much higher with longer interrogation times. Keeping a low contrast loss with high interrogation time will thus demand extensive compensation of all rotational effects. Longer interrogation times also lead to a larger physical package size and will demand wider laser beams and higher powers. They will also need improved mirrors in terms of flatness to avoid the wavefront aberration noise from getting large values.

Fig. 14 compares the total measurement noise of CAI accelerometers with different interrogation times in the frequency domain, assuming that all rotational effects are fully compensated. Sensitivity levels down to 1×10^{-13} m/s^2/$\sqrt{\text{Hz}}$ could be reached, extrapolating interferometer duration up to 60 s. Increasing the interferometry duration beyond this would result in a drop in the sensitivity.

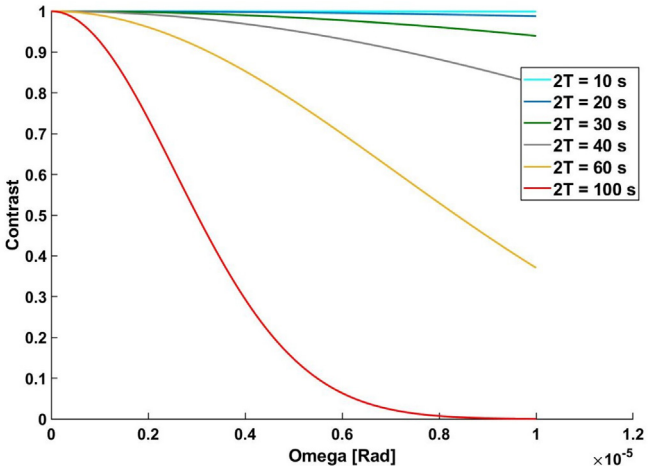

Fig. 13. Long-interrogation-time atom interferometry in space; In all cases, assumptions of the far-future atom interferometry in space (see Table 2) are applied together with a longer interrogation time.

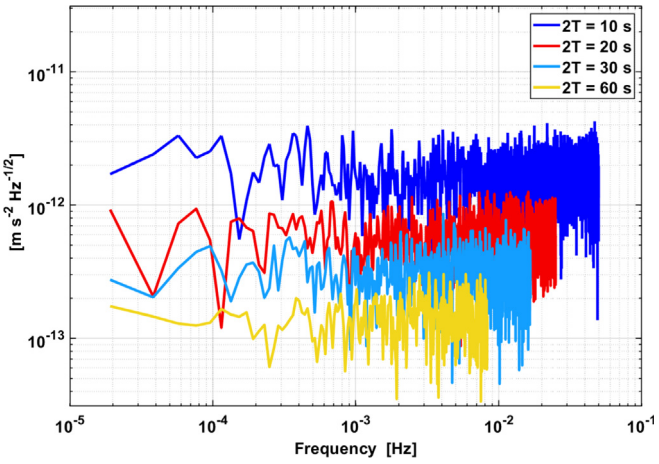

Fig. 14. Long-interrogation-time atom interferometry in space. In all cases, assumptions of the far-future atom interferometry are applied with the difference of having longer interrogation times and a comparable E-ACC in terms of accuracy in higher frequencies. With higher interrogation time, the sensitivity of the instrument will increase according to Eq. (1). However, there is also an increase in several error sources (e.g. contrast loss due to the Coriolis effect). The total noise level is calculated considering the combination of all these effects.

5. Conclusions

Quantum accelerometers are foreseen for future satellite gravity missions. In this study, we develop an in-orbit performance model for a quantum accelerometer onboard future gravity missions, in which we study the impact of various sources of errors on the stability of cold atom interferometers. We investigate their performance under different assumptions about the positioning and rotation compensation method, and we conclude that without an active rotation compensation method which employs an actuator to create a counter-rotation based on the gyro data at each instant in time, the errors will be so large as to prohibit from benefiting from the instrument.

We also show that in the scenario where the CAI accelerometer is placed on the along-track axis, and the rotation is compensated by using an active counter-rotating Raman mirror, the remaining part of the uncompensated rotation will cause a relatively large bias in the CAI accelerometer measurements, compromising the ability of this instrument to act as an absolute inertial instrument. In this scenario, a mathematical calculation and correction of the bias based on the gyro data would reduce the bias by about two orders of magnitude.

We found that the highest sensitivity is achieved by positioning the E-ACC in the center of mass and the CAI

accelerometer beside the E-ACC on the cross-track axis of the satellite. In this scenario, having active counter-rotating Raman mirrors with the rest of the instrument attached to the satellite frame would be sufficient to compensate for the rotational effect. However, for the near and far-future scenarios, counter-rotating the whole sensor would result in factor 3 to 4 improvement in the noise level.

We also discuss current and future advances expected for space-based atom interferometry and investigate their impact on the performance of the CAI accelerometers in different scenarios. First, we consider atom interferometry based on state-of-the-art technology, and we show that a stability level of 5×10^{-10} m/s^2/$\sqrt{\text{Hz}}$ can be achieved. The second scenario is a near-future scenario, where we consider an improved quantum accelerometer based on the technological progress expected in the next 10 to 15 years. An expected sensitivity level of 1×10^{-11} m/s^2/$\sqrt{\text{Hz}}$ to 5×10^{-11} m/s^2/$\sqrt{\text{Hz}}$ is estimated depending on the rotation compensation method.

Then, we consider a far-future scenario and select it as the most efficient quantum accelerometer achievable in the next 20 to 25 years, and we demonstrate that sensitivity in the order of 1×10^{-12} m/s^2/$\sqrt{\text{Hz}}$ could be achieved in this scenario. The major challenges in achieving this sensitivity would be, first, an accurate rotation compensation by a more accurate initialization of the atomic cloud and by employing improved gyros, E-ACC, and Raman mirror actuators with respect to state-of-the-art technology. The other challenge would be an increase in the number of atoms in the atomic cloud to 10^7. This would be necessary to reduce the quantum projection noise, which turns out to be critical at this level of stability. An alternative approach would be to apply a squeezing technique to reduce the QPN by the same magnitude.

Based on our simulation results, we provide a roadmap for advances in atom interferometry that would maximize the performance of future CAI accelerometers, taking into account possible improvements as well as technical challenges. We conclude that for each set of assumptions for the quantum sensor, there is an optimal interrogation time. The optimal interferometry duration are respectively 5 s, 10 s and 20 s for the state-of-the-art, near-future and far-future scenarios. Finally, we discuss the possibility and challenges of having ultra-sensitive atom interferometry for future space missions by considering longer interrogation times in space. Apart from its applications for future satellite gravimetry, this ultra-sensitive quantum sensor could be very attractive for space-based experiments of fundamental physics.

Declaration of Competing Interest

The authors declare that they have no known competing financial interests or personal relationships that could have appeared to influence the work reported in this paper.

Acknowledgments

This work is supported by the Deutsche Forschungsgemeinschaft (DFG, German Research Foundation) Collaborative Research Center 1464 "TerraQ" — 434617780 and Germany's Excellence Strategy — EXC-2123 "QuantumFrontiers" — 390837967, and by the European Union's Horizon 2020 research and innovation programme under grant agreement No 101081775 (CARIOQA-PMP project). This study is also partially supported by SpaceQNav project funded by the Federal Ministry for Economic Affairs and Climate Action (BMWK), Project 50NA2310A. QB and FP acknowledge the support from a government grant managed by the Agence Nationale de la Recherche under the Plan France 2030 with the reference "ANR-22-PETQ-0005". B.T. acknowledges support from the Federal Ministry for Economic Affairs and Energy (BMWi), Project 50RK1957. A. K. acknowledges support by Deutsches Zentrum für Luft- und Raumfahrt e.V. (DLR) for the project Q-BAGS.

References

Abend, S., Gersemann, M., Schubert, C. et al., 2020. Atom interferometry and its applications. In: Rasel, E.M., Schleich, W., Wölk, S. (Eds.), P Int Sch Phys. volume 197, pp. 345–392. doi:10.3254/978-1-61499-937-9-345.

Abrykosov, P., Pail, R., Gruber, T., et al., 2019. Impact of a novel hybrid accelerometer on satellite gravimetry performance. Adv. Space Res. 63 (10), 3235–3248. https://doi.org/10.1016/j.asr.2019.01.034.

Anders, F., Idel, A., Feldmann, P., et al., 2021. Momentum entanglement for atom interferometry. Phys. Rev. Lett. 127, 140402. https://doi.org/10.1103/PhysRevLett.127.140402.

Antoni-Micollier, L., Arnal, M., Gautier, R., et al., 2024. Absolute quantum gravimeters and gradiometers for field measurements. ArXiv e-prints, arXiv:2405.10844.

Antoni-Micollier, L., Carbone, D., Ménoret, V., et al., 2022. Detecting volcano–related underground mass changes with a quantum gravimeter. Geophys. Res. Lett. 49 (13). https://doi.org/10.1029/2022GL097814.

Asenbaum, P., Overstreet, C., Kim, M., et al., 2020. Atom-interferometric test of the equivalence principle at the 10^{-12} level. Phys. Rev. Lett. 125, 191101. https://doi.org/10.1103/PhysRevLett.125.191101.

Aveline, D.C., Williams, J.R., Elliott, E.R., et al., 2020. Observation of Bose-Einstein condensates in an Earth-orbiting research lab. Nature 582 (7811), 193–197. https://doi.org/10.1038/s41586-020-2346-1.

Beaufils, Q., Lefebve, J., Baptista, J.G., et al., 2023. Rotation related systematic effects in a cold atom interferometer onboard a nadir pointing satellite. NPJ Microgr. 9 (1). https://doi.org/10.1038/s41526-023-00297-w.

Becker, D., Lachmann, M.D., Seidel, S.T., et al., 2018. Space-borne Bose-Einstein condensation for precision interferometry. Nature 562 (7727), 391–395. https://doi.org/10.1038/s41586-018-0605-1.

Cheng, B., Wang, Z., Wu, B., et al., 2014. The effects of the non-uniformity of raman laser beams on an atom interferometer. Eur. Phys. J. D 68 (11), 343. https://doi.org/10.1140/epjd/e2014-40698-1.

Chiow, S.-W., Kovachy, T., Chien, H.-C., et al., 2011. 102 $\hbar$ k large area atom interferometers. Phys. Rev. Lett. 107 (13), 130403. https://doi.org/10.1103/PhysRevLett.107.130403.

Daras, I., March, G., Wiese, D., et al., 2023. Next Generation Gravity Mission (NGGM) Mission Requirements Document. Technical Report Earth and Mission Science Division, European Space Agency. https://doi.org/10.5270/ESA.NGGM-MRD.2023-09-v1.0.

Dávila Álvarez, A., Knudtson, A., Patel, U., et al., 2022. A simplified gravitational reference sensor for satellite geodesy. J. Geodesy 96 (10). https://doi.org/10.1007/s00190-022-01659-0.

Deppner, C., Herr, W., Cornelius, M., et al., 2021. Collective-mode enhanced matter-wave optics. Phys. Rev. Lett. 127 (10), 100401. https://doi.org/10.1103/PhysRevLett.127.100401.

Elsen, M., Piest, B., Adam, F., et al., 2023. A dual-species atom interferometer payload for operation on sounding rockets. Microgr. Sci. Technol. 35 (5), 1–14. https://doi.org/10.1007/s12217-023-10068-7.

Flury, J., Bettadpur, S., Tapley, B.D., 2008. Precise accelerometry onboard the GRACE gravity field satellite mission. Adv. Space Res. 42 (8), 1414–1423. https://doi.org/10.1016/j.asr.2008.05.004.

Freier, C., Hauth, M., Schkolnik, V., et al., 2016. Mobile quantum gravity sensor with unprecedented stability. J Phys: Conf Ser 723. https://doi.org/10.1088/1742-6596/723/1/012050.

Freymueller, J., Sanchez, L., (Eds.), 2022. Geodesy for a Sustainable Earth volume 154 of International Association of Geodesy Symposia. Cham: Springer.

Frye, K., Abend, S., Bartosch, W., et al., 2021. The Bose-Einstein Condensate and Cold Atom Laboratory. EPJ Quant. Technol. 8 (1), 1–38. https://doi.org/10.1140/epjqt/s40507-020-00090-8.

Geiger, R., Landragin, A., Merlet, S., et al., 2020. High-accuracy inertial measurements with cold-atom sensors. AVS Quant. Sci. 2 (2), 024702. https://doi.org/10.1116/5.0009093.

Greve, G.P., Luo, C., Wu, B., et al., 2022. Entanglement-enhanced matter-wave interferometry in a high-finesse cavity. Nature 610 (7932), 472–477. https://doi.org/10.1038/s41586-022-05197-9.

Gross, C., Zibold, T., Nicklas, E., et al., 2010. Nonlinear atom interferometer surpasses classical precision limit. Nature 464 (7292), 1165–1169. https://doi.org/10.1038/nature08919.

HosseiniArani, A., Tennstedt, B., Schilling, M., et al., 2022. Kalman-filter based hybridization of classic and cold atom interferometry accelerometers for future satellite gravity missions. In Freymueller & Sanchez (2022). https://doi.org/10.1007/1345_2022_172.

Hosten, O., Engelsen, N.J., Krishnakumar, R., et al., 2016. Measurement noise 100 times lower than the quantum-projection limit using entangled atoms. Nature 529 (7587), 505–508. https://doi.org/10.1038/nature16176.

Humphrey, V., Rodell, M., Eicker, A., 2023. Using satellite-based terrestrial water storage data: A review. Surv. Geophys. 44 (5), 1489–1517. https://doi.org/10.1007/s10712-022-09754-9.

Kasevich, M., Chu, S., 1991. Atomic interferometry using stimulated Raman transitions. Phys. Rev. Lett. 67 (2), 181–184. https://doi.org/10.1103/PhysRevLett.67.181.

Knabe, A., Schilling, M., Wu, H., et al., 2022. The benefit of accelerometers based on cold atom interferometry for future satellite gravity missions. Freymueller & Sanchez (2022). https://doi.org/10.1007/1345_2022_151.

Kupriyanov, A., Reis, A., Schilling, M., et al., 2024. Benefit of enhanced electrostatic and optical accelerometry for future gravimetry missions. Adv. Space Res. 73 (6), 3345–3362. https://doi.org/10.1016/j.asr.2023.12.067.

Lan, S.-Y., Kuan, P.-C., Estey, B., et al., 2012. Influence of the coriolis force in atom interferometry. Phys. Rev. Lett. 108 (9). https://doi.org/10.1103/PhysRevLett.108.090402.

Le Gouët, J., Cheinet, P., Kim, J., et al., 2007. Influence of lasers propagation delay on the sensitivity of atom interferometers. Eur. Phys. J. D 44 (3), 419–425. https://doi.org/10.1140/epjd/e2007-00218-2.

Lecomte, H., Rosat, S., Mandea, M., et al., 2023. Gravitational constraints on the Earth's inner core differential rotation. Geophys. Res. Lett. 50 (23). https://doi.org/10.1029/2023GL104790, e2023GL104790.

Lévèque, T., Fallet, C., Lefebve, J. et al., 2022. CARIOQA: definition of a quantum pathfinder mission. In: Minoglou, K., Karafolas, N., Cugny, B. (Eds.), International Conference on Space Optics — ICSO 2022. SPIE. doi:10.1117/12.2690536.

Lévèque, T., Fallet, C., Mandea, M., et al., 2021. Gravity field mapping using laser coupled quantum accelerometers in space. J. Geod. 95 (15). https://doi.org/10.1007/s00190-020-01462-9.

Lévèque, T., Gauguet, A., Michaud, F., et al., 2009. Enhancing the area of a Raman atom interferometer using a versatile double-diffraction technique. Phys. Rev. Lett. 103, 080405. https://doi.org/10.1103/PhysRevLett.103.080405.

Loomis, B.D., Rachlin, K.E., Wiese, D.N., et al., 2020. Replacing GRACE/GRACE-FO with Satellite Laser Ranging: impacts on Antarctic ice sheet mass change. Geophys. Res. Lett. 47 (3). https://doi.org/10.1029/2019GL085488, e2019GL085488.

Louchet-Chauvet, A., Farah, T., Bodart, Q., et al., 2011. The influence of transverse motion within an atomic gravimeter. New J. Phys. 13 (6), 065025. https://doi.org/10.1088/1367-2630/13/6/065025.

Mandea, M., Dehant, V., Cazenave, A., 2020. GRACE–gravity data for understanding the deep Earth's interior. Remote Sens. 12 (24). https://doi.org/10.3390/rs12244186.

Massotti, L., Siemes, C., March, G., et al., 2021. Next Generation Gravity Mission elements of the Mass Change and Geoscience International Constellation: From orbit selection to instrument and mission design. Remote Sensing 13 (19), 3935. https://doi.org/10.3390/rs13193935.

Merlet, S., Gillot, P., Cheng, B., et al., 2021. Calibration of a superconducting gravimeter with an absolute atom gravimeter. J. Geodesy 95 (5). https://doi.org/10.1007/s00190-021-01516-6.

Merlet, S., Volodimer, L., Lours, M., et al., 2014. A simple laser system for atom interferometry. Appl. Phys. B 117, 749–754. https://doi.org/10.1007/s00340-014-5890-2.

Migliaccio, F., Reguzzoni, M., Batsukh, K., et al., 2019. MOCASS: A satellite mission concept using cold atom interferometry for measuring the Earth gravity field. Surv. Geophys. 40 (5), 1029–1053. https://doi.org/10.1007/s10712-019-09566-4.

Pail, R., Bingham, R., Braitenberg, C., et al., 2015. Science and user needs for observing global mass transport to understand global change and to benefit society. Surv. Geophys. 36 (6), 743–772. https://doi.org/10.1007/s10712-015-9348-9.

Pavlis, N.K., Holmes, S.A., Kenyon, S.C., et al., 2012. The development and evaluation of the Earth Gravitational Model 2008 (EGM2008). J. Geophys. Res.: Solid Earth 117. https://doi.org/10.1029/2011JB008916.

Purkhauser, A.F., Siemes, C., Pail, R., 2020. Consistent quantification of the impact of key mission design parameters on the performance of next-generation gravity missions. Geophys. J. Int. 221 (2), 1190–1210. https://doi.org/10.1093/gji/ggaa070.

Scanlon, B.R., Fakhreddine, S., Rateb, A., et al., 2023. Global water resources and the role of groundwater in a resilient water future. Nat. Rev. Earth Environ. 4 (2), 87–101. https://doi.org/10.1038/s43017-022-00378-6.

Schilling, M., Wodey, E., Timmen, L., et al., 2020. Gravity field modelling for the Hannover 10 m atom interferometer. J. Geod. 94 (12). https://doi.org/10.1007/s00190-020-01451-y.

Tapley, B.D., Watkins, M.M., Flechtner, F., et al., 2019. Contributions of GRACE to understanding climate change. Nat. Clim. Change 9 (5), 358–369. https://doi.org/10.1038/s41558-019-0456-2.

Touboul, P., Metris, S., Le Traon, O., et al., 2016. Gravitation and geodesy with inertial sensors, from ground to space. AerospaceLab. https://doi.org/10.12762/2016.AL12-11.

Trimeche, A., Battelier, B., Becker, D., et al., 2019. Concept study and preliminary design of a cold atom interferometer for space gravity gradiometry. Class. Quant. Grav. 36 (21). https://doi.org/10.1088/1361-6382/ab4548.

Wiese, D.N., Bienstock, B., Blackwood, C., et al., 2022. The mass change designated observable study: Overview and results. Earth Space Sci. 9 (8). https://doi.org/10.1029/2022EA002311, e2022EA002311.

Wöske, F., Kato, T., Rievers, B., et al., 2019. GRACE accelerometer calibration by high precision non-gravitational force modeling. Adv. Space Res. 63 (3), 1318–1335. https://doi.org/10.1016/j.asr.2018.10.025.

Xie, Y., Fan, B., Li, H., et al., 2022. Ground experiment verification and on-orbit prediction of the two-stage cooling at pK level in the Chinese space station. J. Phys. B: At. Mol. Opt. Phys. 55 (20), 205301. https://doi.org/10.1088/1361-6455/ac8e3d.

Zahzam, N., Christophe, B., Lebat, V., et al., 2022. Hybrid electrostatic-atomic accelerometer for future space gravity missions. Remote Sens. 14 (14). https://doi.org/10.3390/rs14143273.